Int. J. Electrochem. Sci., 9 **(2014)** 5352 - 5374

International Journal of
ELECTROCHEMICAL
SCIENCE
www.electrochemsci.org

Electrochemical and Corrosion Behavior of cast Re-containing Inconel 718 Alloys in Sulphuric Acid Solutions and the Effect of Cl^-

Mohammed A. Amin[1,2,*], *Nader El-Bagoury*[1,3], *Murat Saracoglu*[4], *Mohamed Ramadan*[3,5]

[1]Materials and Corrosion Lab, Chemistry Department, Faculty of Science, Taif University, 888 Hawiya, SAUDI ARABIA.
[2]Chemistry Department, Faculty of Science, Ain Shams University, P.O. Box 11566, Abbassia, Cairo, EGYPT.
[3]Casting Technology Lab., Manufacturing Technology Dept., Central Metallurgical Research and Development Institute, CMRDI, P.O. Box 87, Helwan, Cairo, EGYPT.
[4]Faculty of Education, Erciyes University, 38039 Kayseri, Turkey
[5]College of Engineering, University of Hail, Hail, Saudi Arabia
[*]E-mail: maaismail@yahoo.com

Received: 1 April 2014 / *Accepted:* 29 May 2014 / *Published:* 16 June 2014

The effect of Rhenium (Re) additions (2.4, 3.5, and 6%) to a standard Inconel 718 alloy (IN718) on the uniform and pitting corrosion processes of IN718 was studied. Measurements were conducted in 1.0M H_2SO_4 solutions without and with 0.1M, 0.3M, or 0.6M NaCl at 25 ^oC, employing various electrochemical techniques, complemented with SEM/EDS and AFM examinations. The corrosion behavior at equilibrium (corresponding to immersion of samples without polarization) was studied as a function of alloy composition by monitoring the open-circuit potential (OCP), electrochemical impedance spectroscopy (EIS) measured at the corrosion potential (E_{corr}), and by polarization studies around E_{corr} (E_{corr}±250 mV). The anodic behavior of the tested alloys was also studied in 1.0M H_2SO_4 solutions without and with Cl^-, based on potentiodynamic anodic polarization measurements. A potentiostatic technique (current *vs.* time measurements at a given potential) was also employed to access the role of the alloyed Re in the kinetics of pit initiation and growth induced by Cl^-. Experimental findings showed that the rates of the uniform and pitting corrosion processes decreased when Re content increased from 2.5% to 3.5%. However, further increase in alloyed Re content (up to 6%) has resulted in an obvious enhancement in the rates of uniform and pitting corrosion processes. Potentiostatic measurements in presence of Cl^- showed that nucleation of pit (initiated by Cl^- at anodic potentials very close to and beyond the pitting potential, E_{pit}) takes place after an incubation time (t_i). The rate of pit nucleation (t_i^{-1}) increases with increase in Cl^- concentration and applied anodic potential (E_a). The results of potentiostatic measurements also revealed that t_i^{-1} suppressed when Re content in the alloy increased up to 3.5%, but enhanced in presence of 6%Re.

Keywords: IN718 alloys; Alloyed rhenium; Corrosion; H_2SO_4 solutions

1. INTRODUCTION

Inconel is a family of austenitic nickel-chromium-based superalloys [1]. The Inconel family of alloys was first developed in the 1940s by research teams at Wiggin Alloys (Hereford, England), which has since been acquired by SMC [2], in support of the development of the Whittle jet engine.

The INCONEL alloy 718 is one of the high performance, corrosion resistant nickel-chromium alloys, and constitutes 45% of the wrought nickel-based super-alloys [3-7]. The ease and economy, with which this alloy can be fabricated, combined with good tensile, fatigue, creep, and rupture strength, have resulted in its use in a wide range of applications. Examples of these are components for liquid fueled rockets, rings, casings and various formed sheet metal parts for aircraft and land-based gas turbine engines, and cryogenic tankage [8-13].

INCONEL alloy 718 provides good resistance to aqueous corrosion in seawater and is widely used for fasteners and hardware in marine construction. The excellent corrosion resistance is largely due to the Ni-base alloys surfaces protected in aqueous electrolytes or moist air by ultrathin dense oxide/hydroxide films. The films act as an effective barrier to separate the substrate alloys from the corrosive environment and thus protects the substrate alloys from further corrosion processes [14-16]. Therefore, nickel-base alloys exhibit unusual corrosion resistance property in many corrosive environments.

Unfortunately, the passive film does not afford complete protection of the substrate alloys. For instance, in tribocorrosion systems, tribological contact can often damage or even remove the passive film, as a result, exposing the active substrate alloy surface to the corrosive environment, resulting in an anodic dissolution of the alloys. In addition, certain aggressive ions (e.g., Cl^-, Br^-) can also induce passivity breakdown, resulting in various forms of localized corrosion, such as pitting attack and stress corrosion cracking [17-20]. Localized corrosion processes can result in the rapid penetration of a cavity pit or crack into the alloy substrate, thus leading to premature failure. Acid media can also result in corrosion attack.

Considering the potential applications of Ni-base superalloys, and due to the aggressive environments where such alloys are used, the requirement is to have not only high tensile and creep strength but also high corrosion resistance. Thus, the corrosion resistance of Inconel 718 in aqueous solutions is an important issue to study, particularly the generalized corrosion attack occurring in acid media. In addition, the literature contains very few studies about the corrosion behavior, corrosion rate, and anodic behavior in acid media of these materials.

The objective here is to study the effect of Re (2.4, 3.5 and 6% Re), as an alloying element, on the corrosion behavior (including uniform and pitting corrosion processes) of IN718 alloy in H_2SO_4 solutions without and with different concentrations of Cl^-. Measurements were carried out with the use of various electrochemical measurements, including: (i) monitoring OCP, (ii) EIS measured at E_{corr}, (iii) polarization studies around E_{corr} (E_{corr}±250 mV), (iv) linear sweep voltammtery, and (v) potentiostatic (current/time) measurements as a function of electrolyte composition at different applied anodic potentials.

An independent method of chemical analysis (ICP-AES) was also employed to determine the concentration of Ni^{2+} (C_{Ni}^{2+} in solution is taken as a measure for the corrosion rate) in solution due to uniform and pitting corrosion processes of the tested alloys in H_2SO_4 solutions. The aim of the ICP method is to clarify the effect of Re on the rate of uniform and pitting attack and to confirm electrochemical measurements.

Finally, morphologies and topographical characterizations of the corroded surfaces of the tested alloys were investigated by SEM and AFM as a function of Re content in the tested alloy.

2. EXPERIMENTAL

2.1. Chemical Composition and Melting Process

The chemical compositions of the tested alloys, namely Re-containing IN718 alloys, are presented elsewhere [21].

These alloys were cast as cylindrical rods for the electrochemical tests. These rods were machined carefully and mounted in polyester resin after the electric contact, with special care taken to prevent the presence of crevices. The exposed area was ~ 1.0 cm^2. Before each run, the samples were wet ground with 600-grit silicon carbide (SiC) paper, washed in distilled water, and immersed in the electrochemical cell. The samples were then subjected to open circuit conditions until a steady state potential was reached. This procedure was accomplished in 24hrs and the potential value obtained was considered the corrosion potential (E_{corr}).

All chemical and electrochemical tests were performed in 1.0 M H_2SO_4 solutions without and with 0.1M, 0.3M, or 0.6M NaCl, as the corrosive medium, prepared with analytical grade chemicals and doubly distilled water. The solutions were naturally aerated and the temperature was held at 25 ◦C using a temperature control water bath. A conventional electrochemical cell was used, consisting of a platinum counter electrode and Ag/AgCl reference electrode. A Luggin–Haber capillary was also included in the design. The tip of the Luggin capillary is made very close to the surface of the working electrode to minimize IR drop.

In order to avoid Cl^- diffusion in the cell, the reference electrode was connected to the working electrode through a bridge filled with the solution under test, the capillary tip of the bridge was very close to the surface of the working electrode to minimize the IR drop. In addition, Cl^- ion was potentiometrically detected in the test solution before and after each polarization experiment using an Ag/AgCl selective electrode and a standard solution of $AgNO_3$ and a HANNA pH-meter model pH 211. The aim is to make sure that the corrosion attack originates only from H_2SO_4. In all cases, the obtained results revealed the absence of Cl^- ion in the tested solution.

The electrochemical cell was connected to a potentiostat; Autolab frequency response analyzer (FRA) coupled to an Autolab Potentiostat/Galvanostat (PGSTAT30) with FRA2 module connected to a personal computer.

Open circuit potential (OCP) *vs.* time (up 24 hrs), EIS measured at the respective E_{corr}, and polarization measurements around E_{corr} (E_{corr} ± 250 mV) are the electrochemical techniques used to study the corrosion behavior of Re-containing IN718 alloys in these solutions at the OCP. On the other hand, potentiodynamic anodic polarization, current density (*j*) *vs.* the potential of the working

electrode (*E vs.* Ag/AgCl), and potentiostatic (current/time transients) measurements were employed for investigating the anodic behavior, including passivity (passive layer formation and growth) and breakdown of passivity induced by Cl^- (kinetics of pit nucleation and propagation), of such alloys.

Impedance measurements were carried out using AC signals of amplitude 5 mV peak to peak at the open circuit potential in the frequency range 100 kHz to 1.0 mHz. For polarization studies around E_{corr}, the potential of the working electrode is varied from $(E_{corr}\text{-}0.25)V_{Ag/AgCl}$ to $(E_{corr}\text{+}0.25)V_{Ag/AgCl}$ using a scan rate of 1.0 mV s^{-1}.

The potentiodynamic curves were recorded by changing the electrode potential automatically from -1.5V(Ag/AgCl) to the required anodic potential at a potential scan rate of 1.0 mV s^{-1}.

The order of performing electrochemical measurements was: (i) Chronopotentiometry (zero current); OCP *vs.* time (up to 24hrs) (*non-destructive technique*), followed by (ii) impedance measurements at E_{corr} (*non-destructive technique*), and (iii) polarization measurements around E_{corr} ($E_{corr} \pm 250$ mV) (*destructive technique*). As the later is a destructive technique, the cell is cleaned, the test solution is replaced by a fresh one, and a cleaned set of electrodes was used for (iv) potentiodynamic anodic polarization measurements.

Finally, potentiostatic current *vs.* time measurements were carried out using a two step procedure, namely: the working electrode was first held at the starting potential for 60s to attain a reproducible electroreduced electrode surface. Then the electrode was held at constant anodic potential (E_a), where the anodic current was recorded as a function of time.

Morphologies and topographical characterizations of the corroded surfaces of the tested alloys, after the potentiodynamic anodic polarization measurements in 1.0 M H_2SO_4 solutions at 25 ^oC have been completed, were characterized using an Analytical Scanning Electron Microscope JEOL JSM 6390 LA and AFM (Veeco Multimode 8). The compositions of such corroded surfaces were determined using ZAF software to quantify the energy-dispersive X-ray spectroscopy (EDS) spectra obtained by an EDS attachment (JEOL EDS EX-54175JMU) on the JEOL SEM.

The resultant solutions were used for evaluation of the corrosion rate via determination of Ni^{2+} released. The amount of nickel released into the corrosive medium was taken as a measure of the corrosion rate. In this respect, an independent method of chemical analysis, namely ICP-AES was employed, using Perkin–Elmer Optima 2100 Dual View inductively coupled plasma atomic emission spectrometry (ICP-AES) instrument connected with AS 93 Plus autosampler.

3. RESULTS AND DISCUSSION

3.1. Corrosion behavior at equilibrium

3.1.1. Rest potential vs. time measurements

Figure 1 shows the variation with time (up to 24hrs) the rest potential of IN718, IN718-2.4%Re, IN718-3.5%Re and IN718-6%Re alloys in 1.0 M H_2SO_4 solution at 25 ^oC. In the first moments of immersion, the rest potential of each electrode moves towards less negative values due to the initial formation and growth of the passive oxide film. The potential *vs.* time profile of IN718-6%Re alloy is clarified as shown in the insert of Fig. 1.

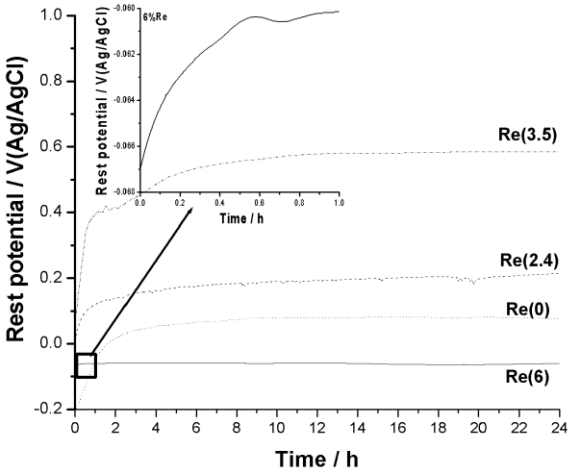

Figure 1. Rest potential *vs.* time (up to 24hrs) curves recorded for IN718, IN718-2.4%Re, IN718-3.5%Re and IN718-6%Re alloys in 1.0 M H_2SO_4 solution at 25 ^oC.

In all cases after the initial rise in the rest potential, a certain constant potential value (steady-state potential) is attained. This value corresponds to, as will be shown later in section 3.1.3, the free corrosion potential (E_{corr}) of the tested alloy.

The steady-state rest potential (i.e., E_{corr}) is made more positive with increase in Re content (except for 6%Re). In addition, the slope of the linear rise in the rest potential (dE/dt), which is a measure for the passivation rate [22], increases following the order: IN718-6%Re < IN718 < IN718-2.4%Re < IN718-3.5%Re. These findings reveal that the tested alloys tend to passivate in H_2SO_4 solution, and the rate of passivation depends on Re content.

Comparison of IN718 alloy (that is free from Re) with that contains 6%Re (i.e., IN718-6%Re) shows that E_{corr} of the latter is always more negative. In addition, IN718-6%Re alloy recorded the lowest passivation rate among the tested alloys. These findings reflect a more active corrosion surface of IN718-6%Re alloy when compared with IN718. This difference could be related to the acceleration influence (harmful effect) of the alloyed Re (see later). The more negative E_{corr} of alloy IN718-6%Re suggests that the presence of this high percentage (6%) of alloyed Re influences the kinetics of the cathodic reaction.

On the other hand increasing the percentage of the alloyed Re from 2.4 to 3.5%, shifts E_{corr} towards the less negative values, suggesting a predominant influence of Re on the anodic reaction.

Based on the above arguments, IN718-6%Re alloy is expected to be subjected to corrosion more than IN718 alloy itself, and the latter is less corrosion resistant *vs.* IN718-2.4%Re and IN718-3.5%Re alloys, see later.

3.1.2. EIS measurements

To glean the effect of alloyed Re on the uniform corrosion behaviour of IN718 alloy, we performed impedance measurements for each alloy at the respective E_{corr} value. The obtained impedance data are collected in Fig. 2.

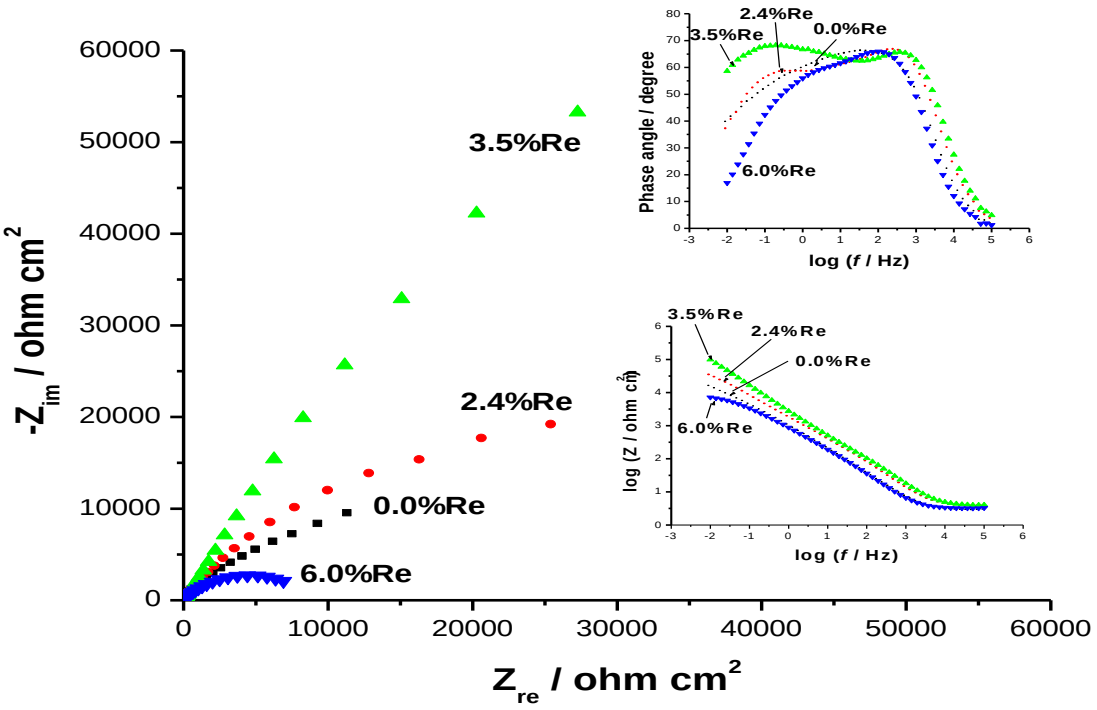

Figure 2. Complex-plane impedance plots recorded for IN718, IN718-2.4%Re, IN718-3.5%Re and IN718-6%Re alloys in 1.0 M H_2SO_4 solution at the respective corrosion potentials at 25 ^oC. Inserts – the corresponding phase angle and total impedance *vs.* log (*f*) plots.

Analysis of the impedance data with a suitable semicircle showed that IN718-6.0%Re alloy exhibited much lower impedance (R_{ct} ~ 8000 Ω cm^2) than the other tested alloys (R_{ct} ~ 24000 Ω cm^2, 50000 Ω cm^2, and 85000 Ω cm^2 for IN718, IN718-2.4%Re, and IN718-3.5%Re alloys, respectively). The significantly reduced impedance recorded for IN718-6.0%Re alloy afforded markedly faster charge-transfer (corrosion) process that occurred on the surface of such alloy. The reverse is true for IN718-3.3%Re alloy, which exhibited the highest R_{ct} value among the tested alloys. It seems that the presence of a higher content of alloyed Re (6.0%) in IN718 alloy is harmful; it enhances the electron transfer in the system resulting in a lower semi-circle diameter which means a decrease of the charge transfer resistance at electrode surface.

3.1.3. Tafel polarization measurements

The influence of alloyed Re on the kinetics of the cathodic and anodic processes of IN718 alloy in 1.0 M H_2SO_4 solution was established on the basis of Tafel polarization measurements, Fig. 3.

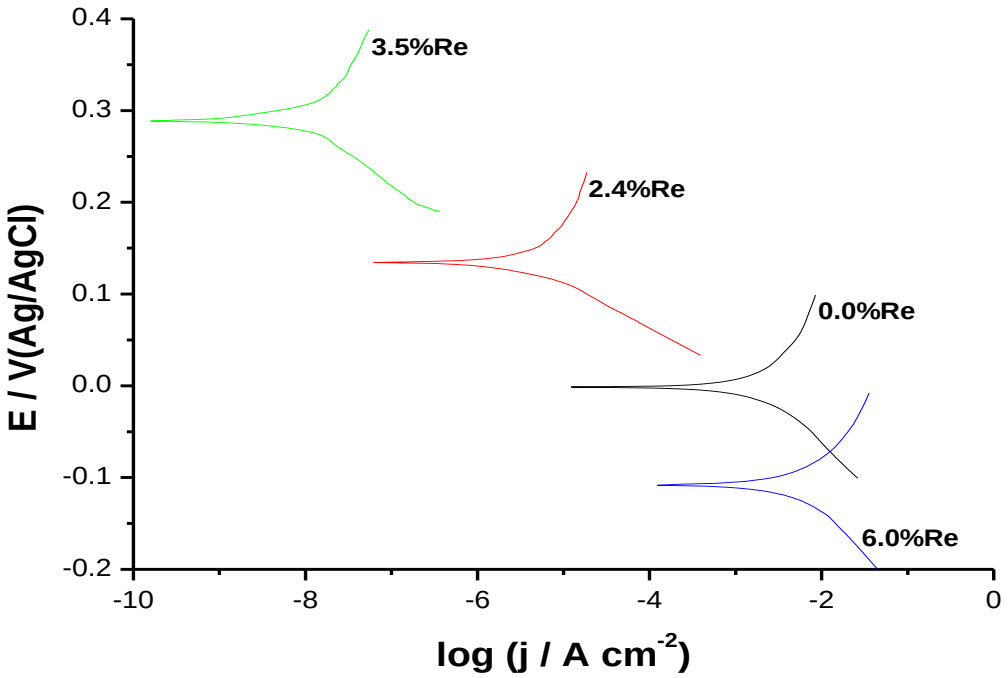

Figure 3. Cathodic and anodic polarization (Tafel) plots recorded for IN718, IN718-2.4%Re, IN718-3.5%Re and IN718-6%Re alloys in 1.0 M H_2SO_4 solution at a scan rate of 1.0 mV s^{-1} at 25 ^oC.

It follows from Fig. 3 that upon alloying IN718 with Re, significant changes in the profile of the Tafel plots, particularly in the location of E_{corr} and in the magnitudes of the overpotentials of both the anodic and cathodic processes, result.

Such changes, considering IN718-2.4%Re and IN718-3.5%Re alloys, are significant upward (anodic) displacement in E_{corr}. The reverse was observed when IN718 alloyed with a higher percentage (6%) of Re, yielding IN718-6%Re alloy; a marked downward (cathodic) shift in both E_{corr} has occurred. In all cases the displacement in E_{corr} observed in the Tafel plots (Fig. 3) follows the same direction of the steady-state potential displacement recorded by means of rest potential *vs.* time plots (Fig. 1). This confirms that the steady-state potential shown in Fig. 1 corresponds, or better "refers", to E_{corr}.

In all cases it has been shown that, except for IN718-6%Re alloy, the cathodic and anodic overpotentials increase (i.e., the rates of the cathodic and anodic reactions are retarded) upon alloying IN718 with 2.4%Re and 3.5%Re.

3.1.3.1. Tafel extrapolation method for monitoring rates of corrosion and analysis of Tafel plots

Extrapolation of Tafel lines is one of the most popular DC techniques for estimation of corrosion rate. However, it is obvious from the polarization plots of the present work (Fig. 3) that accurate evaluation of the corrosion current density, j_{corr}, and hence the corrosion rate, from anodic branches, and therefore the anodic Tafel slope (β_a), is impossible. This is because the anodic

polarization curves of Fig. 3 do not exhibit linear *E vs.* log *j* relationship (Tafel behavior), which in turn prevents linear extrapolation to the corrosion potential, E_{corr}.

The deviation of the anodic branch from the Tafel behaviour may be attributed to corrosion, passivation and roughening of the anode surface, as will be shown later and fully discussed during studying the anodic behaviour of such alloys (section 3.2).

However, the cathodic branches of Fig. 3 are under activation control and exhibits linearity in accord with Tafel relationship.

It has been shown that in the Tafel extrapolation method, use of both the anodic and cathodic Tafel regions is undoubtedly preferred over the use of only one Tafel region [23].

In the present work some mathematical treatments, based on the work of McCafferty [23], were performed on the experimental anodic branches, which deviate from the Tafel behavior, to generate what is called "a calculated anodic Tafel region", as follows.

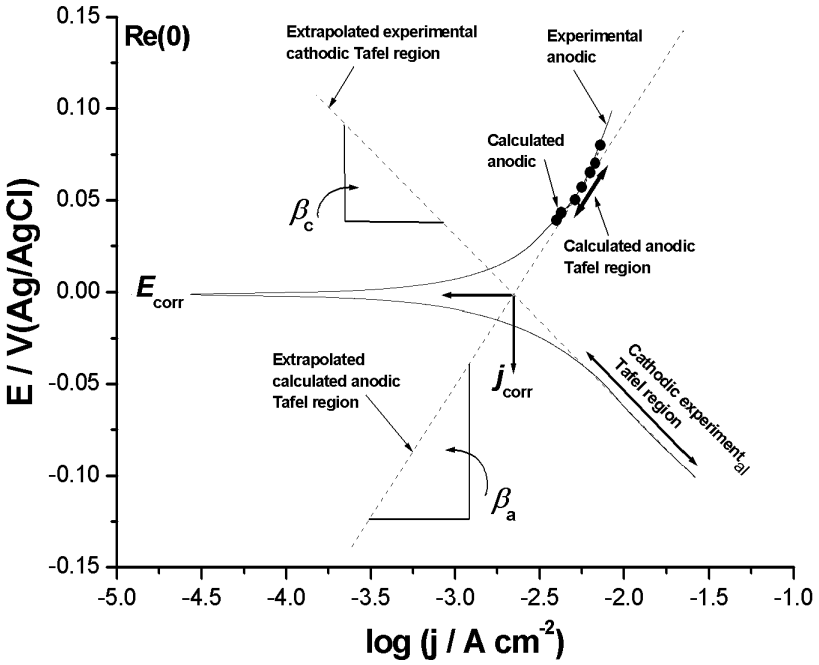

Figure 4. Analysis of the cathodic and anodic polarization (Tafel) plots recorded for IN718 alloy in 1.0 M H_2SO_4 solution at a scan rate of 1.0 mV s^{-1} at 25 ^oC.

The Tafel line of the cathodic polarization curve is first extended, since it exhibits a linear Tafel region, to electrode potentials below the corrosion potential, and then the anodic current density, j_a, is calculated from [23]:

$$J_a \text{ (net experimental)} = j_a - |j_c| \quad (1)$$

where the subscripts a and c refer to the anodic and cathodic direction, respectively. $|j_c|$ is the cathodic current density.

Thus, the calculated anodic current density, j_a, is the sum of the experimentally observed anodic current density and the extrapolated cathodic current density [23]. Such mathematical treatments were performed for the four tested alloys; inspect Fig. 4 as a representative example.

The anodic Tafel slope may now be estimated accurately by extrapolating the calculated anodic Tafel region back to E_{corr}, as shown in Fig. 4.

Table 1 collects, as a function of alloy composition, the electrochemical kinetic parameters derived from such mathematical treatments, together with the rates corrosion calculated from Tafel extrapolation method.

Table 1. Electrochemical parameters and corrosion rates, derived from Tafel polarization measurements, together with the rates of corrosion evaluated from ICP-AES method of chemical analysis recorded for IN718, IN718-2.4%Re, IN718-3.5%Re and IN718-6%Re alloys after 24h of immersion in 1.0 M H_2SO_4 solution at 25 ^oC.

Tested alloy	E_{corr} / V	$(j_{corr})_{Tafel}$ / mA cm^{-2}	β_a / V dec^{-1}	$-\beta_c$ / V dec^{-1}	υ_{Tafel} / mpy	$(j_{corr})_{ICP}$ / mA cm^{-2}	υ_{ICP} / mpy
IN718	-0.01	2.19	0.123	0.093	876	2.04	815
IN718-2.4%Re	0.135	3.63 x 10^{-3}	0.086	0.05	1.45	2.9 x 10^{-3}	1.1
IN718-3.5%Re	0.289	1.07 x 10^{-5}	0.106	0.069	4.28 x 10^{-3}	0.98 x 10^{-5}	3.88 x 10^{-3}
IN718-6%Re	-0.11	5.62	0.114	0.103	2248	5.30	2105

The influence of Re on the rate of uniform corrosion of IN718 alloy was confirmed chemically using inductively coupled plasma-atomic emission spectroscopy (ICP-AES). This method of chemical analysis involved determination of Ni^{2+} ions released in solution after 24h of immersion as a function of alloy composition.

In ICP measurements, known aliquots of the solution containing Ni^{2+} ions were withdrawn for each alloy after 24h of immersion (the same time adopted in rest potential *vs.* time measurements, Fig. 1) in 1.0 M H_2SO_4 solution and analyzed. The rates of corrosion (υ) were expressed as mg cm^{-2} h^{-1} (i.e., mass, in mg, of Ni dissolved as Ni^{2+} per unit area per unit time). The numerical values of the corrosion rates were converted into the corresponding corrosion current density (j_{corr}) values, Table 1, using Faraday's law [24].

All the recorded corrosion current density values obtained from Tafel extrapolation method and the ICP method of chemical analysis are converted into corrosion rates (in mpy) (milli-inches/year; the penetration rate of corrosion through a metal), using Eq. (2) [24]:

$$\upsilon \text{ (mpy)} = (1.288 \times 10^5) \times \{(j_{corr})(E_w) / (d)(A)\} \quad (2)$$

Where j_{corr} is the corrosion current density in (A cm^{-2}), E_W is the equivalent weight in grams/equivalent, d is the density (in g cm^{-3}), and A is the sample area in cm^2. For the tested Ni-base super alloy, E_w = 25.41 g/equiv. [24] and d = 8.17 g cm^{-3} (see Practice G1 for density values for many metals and alloys used in corrosion testing). The calculated corrosion rate values, as shown in Table 1, were found to be 815, 1.1, 3.88 x 10^{-3} and 2105 mpy for IN718, IN718-2.4%Re, IN718-3.5%Re and IN718-6%Re alloys, respectively. Such rates of corrosion agree and go parallel with those calculated from Tafel extrapolation method. These findings confirm the validity of the Tafel extrapolation method for monitoring rates of corrosion.

Based on the data presented in Table 1, it can be concluded that the experimental findings of chemical and electrochemical measurements revealed that the uniform corrosion rate of the studied alloys enhances in the order: IN718-3.5%Re < IN718-2.4%Re < IN718 < IN718-6%Re.

3.2. Anodic behviour of IN718-Re alloys in 1.0M H_2SO_4 solutions

The anodic behavior of the tested alloys was studied in 1.0 M H_2SO_4 solutions based on the linear sweep voltammetry technique (LSV), Fig. 5. In all cases, the potentials were swept starting from a cathodic potential of -1.5 V *vs.* SCE in the anodic direction at a scan rate of 1.0 mV s^{-1} at 25 ^oC. Before each polarization experiment, the electrode was allowed to corrode freely for a period of 4 h. After this time a steady state open circuit potential, OCP, corresponding to the corrosion potential (E_{corr}) of the working electrode, was obtained.

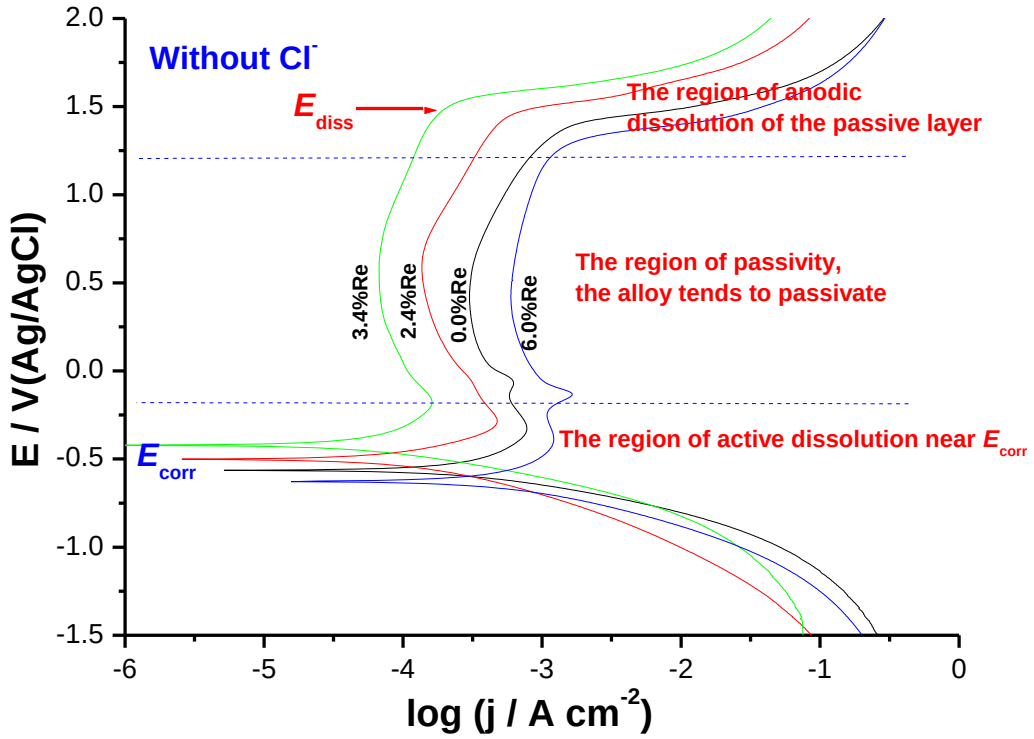

Figure 5. Potentiodynamic anodic polarization curves recorded for the tested alloys in 1.0 M H_2SO_4 solution at a scan rate of 1.0 mV s^{-1} at 25 ^oC, as a function of alloyed Re content.

Experimental polarization curves similar to those depicted in Fig. 5 were obtained in our previous study during corrosion research studies on a Ni-base super alloy in sulphuric acid solutions as a function of solution heat treatments [25].

It follows from Fig. 5 that on positive going scan, the cathodic current density decreases gradually reaching the lowest value at the corrosion potential, E_{corr}, (E_{corr}; close to that obtained from the free corrosion behaviour, rest potential *vs.* time measurements).

The anodic excursion span exhibits an active dissolution region near E_{corr} due to the anodic dissolution of Ni [25]. The kinetics of the anodic dissolution of Ni in acid solutions involves uniform dissolution with the reaction path [26]:

$$Ni + H_2O \leftrightarrow NiOH + H^+ + e^- \quad (3)$$

$$NiOH + H^+ \leftrightarrow Ni^+ + H_2O \quad (4)$$

$$Ni^+ \leftrightarrow Ni^{2+} + e^- \quad (5)$$

The above reaction mechanism considers the water adsorption process in the mechanism of electrooxidation [26].

On the negative side of the polarization curves, the H_3O^+ reduction (reaction 6) is the main reaction occurring on the electrode surface.

$$2H_3O^+ + 2e^- \leftrightarrow 2H_2O + H_2 \quad (6)$$

The overall chemical reaction is the sum of the two half-cell reactions (5) and (6):

$$2Ni^+ + 2H_3O^+ \leftrightarrow 2Ni^{2+} + 2H_2O + H_2 \quad (7)$$

The active dissolution region is followed by a region of passivity; the tested alloys tend to passivate to an extent depending on the alloyed Re content. Within this region, as the potential is made more positive, the current density decreases as a result of corrosion products and/or metal oxides layers formation on the alloy surface. Such layers possess some protective influence and reduce the active dissolution of the alloy (passivation). These results demonstrate that the oxide film is stable in this range of potential, and accordingly a very low current (designated here as the passive current, j_{pass}) results.

Further inspection of Fig. 5 reveals that the value of j_{pass} (at any given anodic potential within the region of passivity) varies with the chemical composition of the tested alloy. The inconel alloy with 3.5%Re recorded the lowest j_{pass} values among the tested alloys, and that is alloyed with 6%Re provided us with the highest j_{pass} value. These results go parallel with the experimental findings of the uniform corrosion measurements, Figs. 1-3.

Further increase in potential caused significant changes in the passive region, the current rose steeply and almost linearly with potential. This happened at a certain critical potential value, designated here as the dissolution potential (E_{diss}). This indicates that the formed passive films do not afford complete protection of the substrate alloy, and the alloy dissolution continues.

3.2.1. Morphologies and topographies of the surfaces of the tested alloys corroded at the rest potential

Figure 6 shows surface morphologies and chemical compositions of the corroded surfaces of Re-free IN718, IN718-2.4%Re, and IN718-6.0%Re alloys after the potentiodynamic anodic polarization experiments described in Fig. 5 have been completed.

It is seen that the corrosion process has preferentially occurred in the interdendritic regions rather than in the dendrites of γ phase, as the corrosion products were only found in the interdendritic zones. This could be explained, as will be shown later on, on the basis that alloyed Re distributes itself in the microstructure of the investigated alloys, then segregates preferentially into γ dendrites. This increases the volume fraction of γ dendrites at the expense of interdendritic regions [21,27,28], and the corrosion resistance of the tested alloys subsequently enhanced.

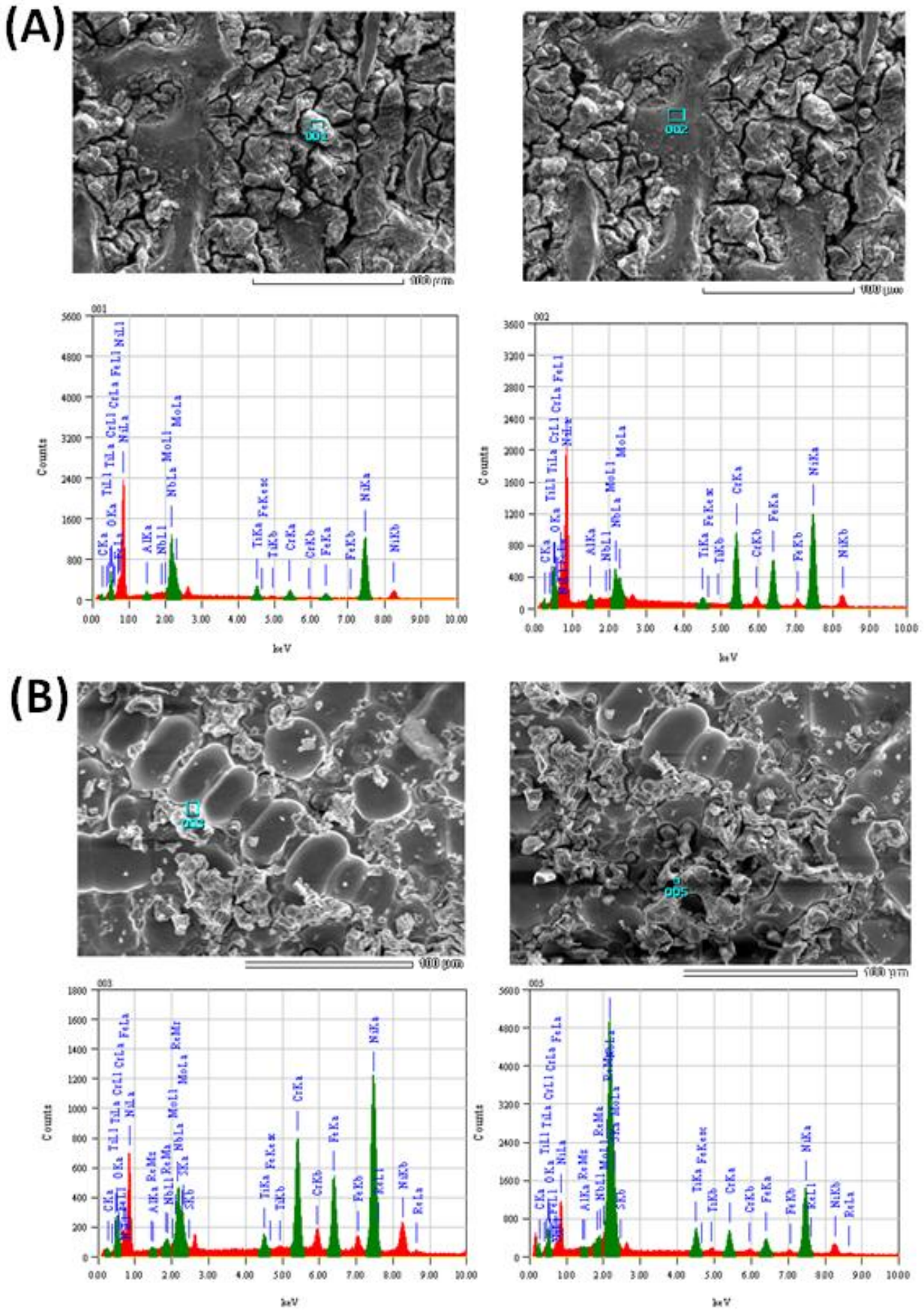
(A)
(B)
Counts
keV

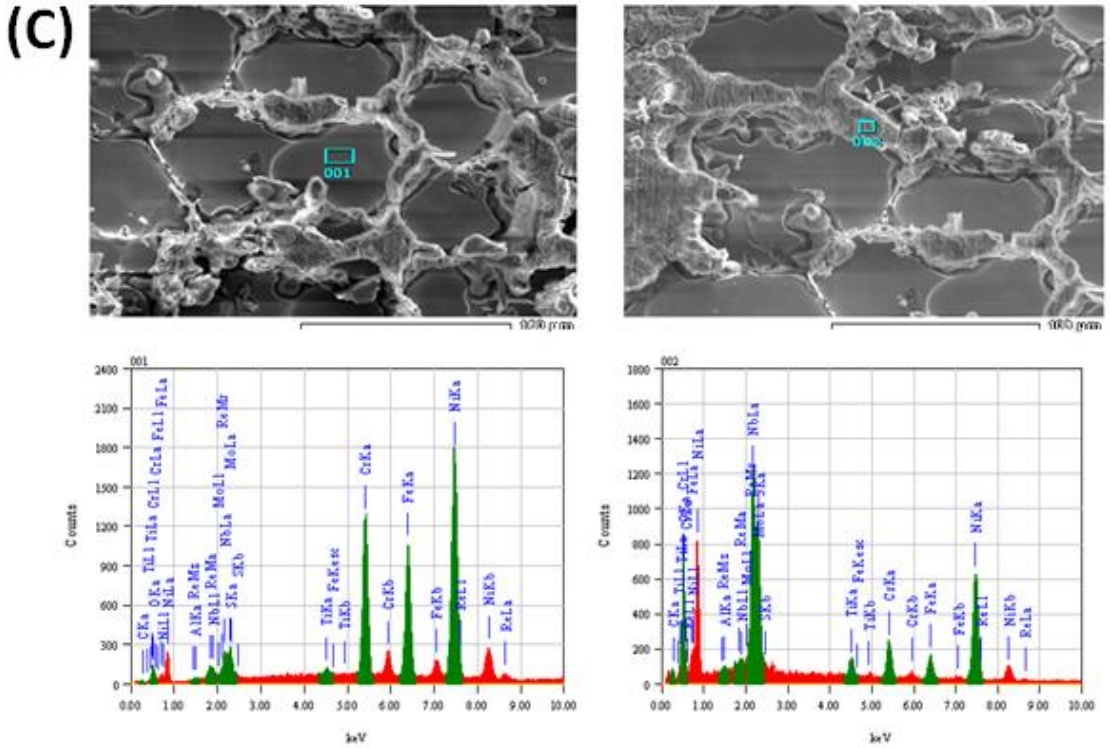

Figure 6. Surface morphologies and chemical compositions (SEM/EDS examinations) of the corroded surfaces of **(A)** IN718 alloy, **(B)** IN718-2.4%Re alloy, and **(C)** IN718-6.0%Re alloy, after the completion of the potentiodynamic anodic polarization experiments depicted in Fig. 5.

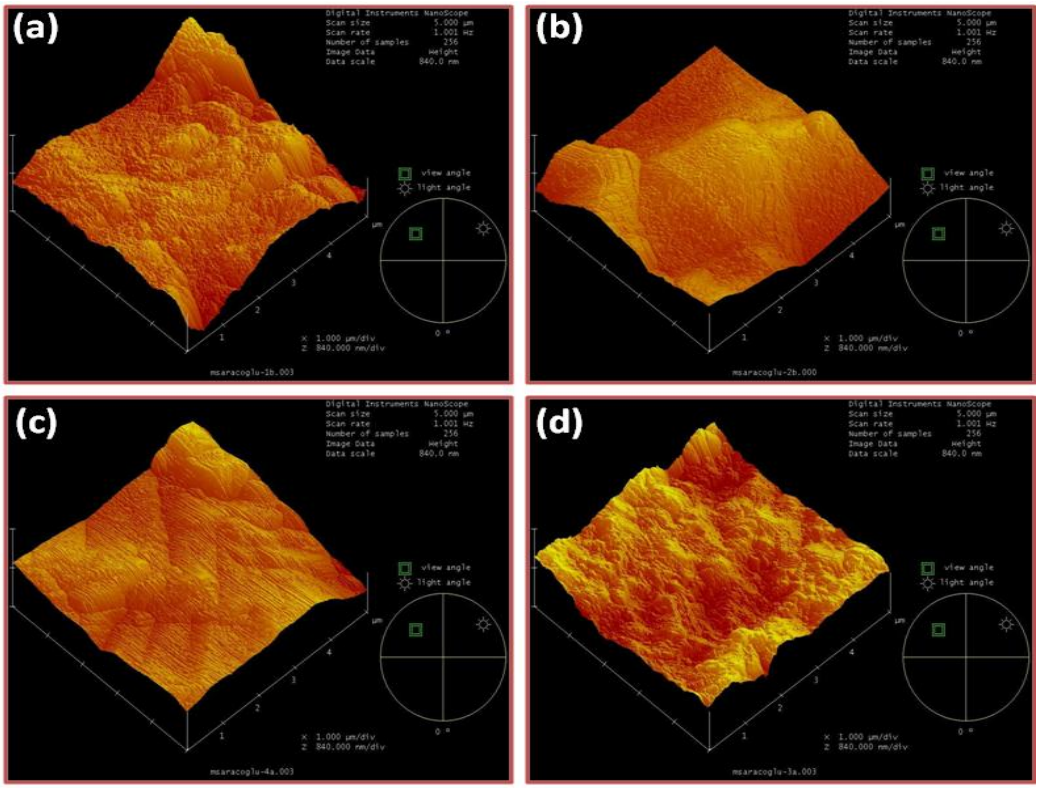

Figure 7. 3D AFM images recorded for the corroded surfaces (after the potentiodynamic polarization run, shown in Fig. 5, has been completed) of **(a)** IN718 alloy; **(b)** IN718-2.4%Re alloy; **(c)** IN718-3.5%Re alloy; **(d)** IN718-6.0%Re alloy.

AFM examinations were also carried out under the same experimental conditions, Fig. 7, to access surface roughness as a function of alloy composition, and to support SEM examinations. It is shown in Fig. 7 that the recorded images are all rough, and the degree of surface roughness varies according to Re content. Reduction of the roughness of the corroded surface enhances on going from Re-free In718 alloy to 3.5% Re-containing In718 alloy, as shown in images a-c.

Here again, 6.0% Re-containing In718 alloy, image d, recorded the highest roughness among the others. These findings confirm the results of electrochemical measurements, and go parallel with SEM examinations, Fig. 6.

To further confirm these results, the mean roughness factor (R_a) was determined from the respective images. The calculated R_a values showed that the roughness of the corroded surface of IN718 decreased from 249.55 nm to 138.7 and 89.254 nm for the corroded surfaces of IN717-2.4%Re and IN717-3.5%Re, respectively, then increased to 278.952 nm for the corroded surface of IN718-6.0%Re alloy.

3.3. Pitting corrosion studies

3.3.1. Effects of Cl^- addition

3.3.1.1. Potentiodynamic anodic polarization measurements

The aggressive influence of Cl^- (0.6M) on the anodic polarization behaviour of our tested IN718 alloys was also studied, and the results obtained are depicted in Fig. 8. Similar findings were obtained in presence of 0.1M and 0.3M Cl^- (data not shown here).

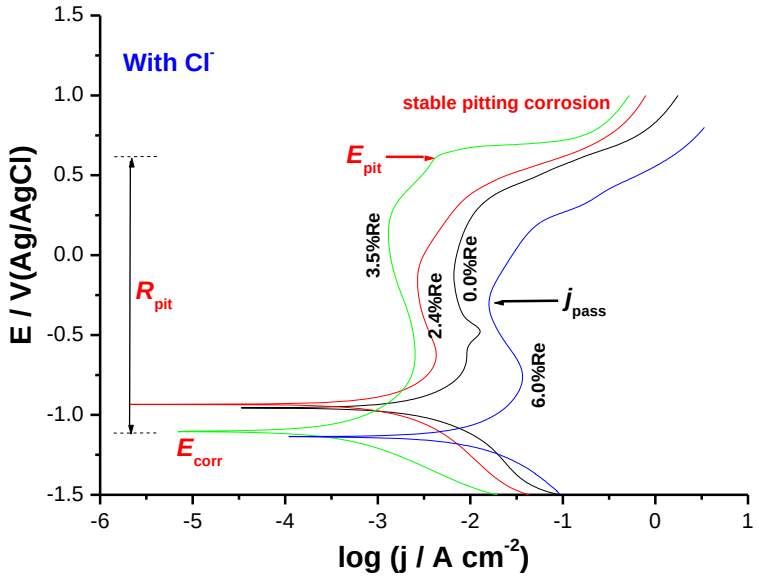

Figure 8. Potentiodynamic anodic polarization curves recorded for the tested alloys in (1.0 M H_2SO_4 + 0.6 M NaCl) solution at a scan rate of 1.0 mV s^{-1} at 25 ^oC.

It is obvious for all of the tested alloys that, as compared with the values of j_{pass} obtained without Cl^- (Fig. 5), the j_{pass} value increases, at any given potential, in presence of Cl^-, reflecting the aggressiveness of Cl^- towards the passivity of the tested alloys. These findings could be attributed to general weakness and thinning of the passive film as a result of Cl^- adsorption (assisted by the applied electric field) on the passive oxide surface. This adsorption is expected to enhance as the potential (the applied electric field) made more positive, as evidenced from the obvious increase in j_{pass} with potential. Here again, the alloy with 3.5%Re recorded the lowest j_{pass} values among the others, while that alloyed with 6.0%Re presented the highest j_{pass} values.

Passivity persists as the potential is increased to a value exceeding a certain critical potential value, known as the pitting potential (E_{pit}). The relative insensitivity of current to increasing potential (characteristic of the passive region) changes abruptly as passivity breaks down at E_{pit}, where a strong potential dependence of the current emerges and stable pitting ensues.

The pitting attack is stabilized by the delocalized development of aggressive conditions as the result of metal cation hydrolysis and migration of the aggressive anion [29]. The increase in current with potential beyond E_{pit} reflects an increase in pitting corrosion susceptibility. The increase in pitting susceptibility with increase in potential could be explained on the basis that increasing the applied potential increases the active sites available for pit nucleation [30]. Moreover, an increase in the applied potential may increase the electric field across the passive film and therefore enhances the adsorption of the aggressive Cl^- anions on the passive electrode surface [29]. Previous studies, based on EDS and XPS examinations, also revealed increased adsorption of Cl^-[31], SCN^- [29], $S_2O_3^{2-}$ [32] and ClO_3^- and ClO_4^- anions [33] with increase in the applied anodic potential on the passivated Al and Zn surfaces.

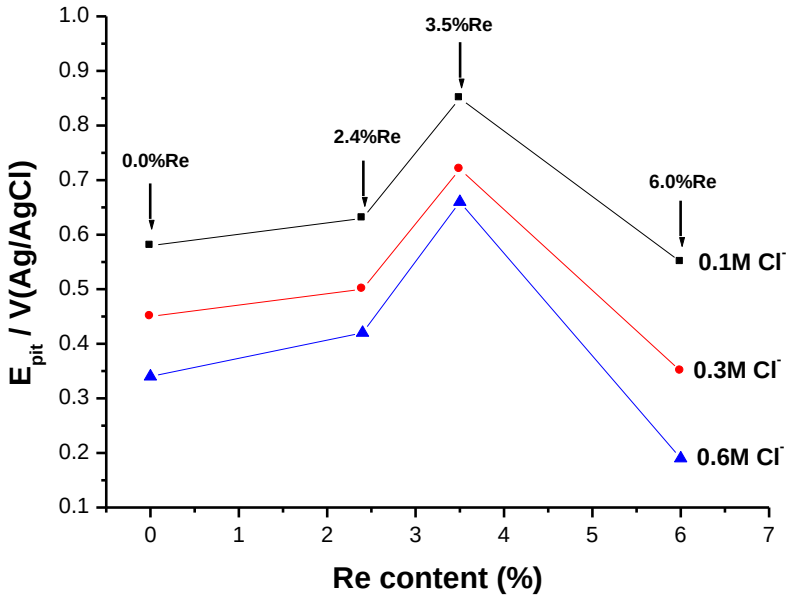

Figure 9. Dependence of the pitting potential (E_{pit}), recorded for the tested alloys in 1.0 M H_2SO_4 solutions containing different concentration of Cl^- at room temperature, on the percentage of alloyed Re content.

Figure 9 represents the variation of E_{pit} values with the Re content, as a function of Cl^- concentration. It is seen that, for all samples, an increase in C_{Cl^-} shifts E_{pit} in the more negative (active) direction, corresponding to decreased resistance to pitting corrosion. It is clear from Fig. 9 that, at any given concentration of Cl^-, the values of E_{pit} increase following the order: (IN718 alloy-3.5%Re) > (IN718 alloy-2.4%Re) > (IN718 alloy) > (IN718 alloy-6.0%Re). These findings indicate that the pitting corrosion resistance of the four samples decreases in the same sequence.

It seems therefore that the presence of alloyed Re increases the pitting corrosion resistance of our Inconel in such aggressive solutions. This increase in the pitting corrosion resistance of (IN 718 alloy-Re) alloys enhances with Re content up to 3.5%, then obviously decreases (even below the Re free-Inconel 718 alloy) upon alloying it with 6.0%Re. These results suggest that the Inconel alloy alloyed with 3.5%Re is the most effective alloy among the other tested alloys in resisting the aggressive pitting attack of Cl^-.

Another important parameter in determining pitting corrosion susceptibility is what is called "pitting corrosion resistance, R_{pit} ($R_{pit} = |E_{corr} - E_{pit}|$)", expressed in volts. A higher R_{pit} value refers to a higher resistance against pitting corrosion [29,34,35]. Here again, the alloy with 3.5%Re recorded the highest R_{pit} value, at any given Cl^- concentration, while that alloyed with 6.0%Re recorded the lowest value for R_{pit}, as shown in Fig. 10.

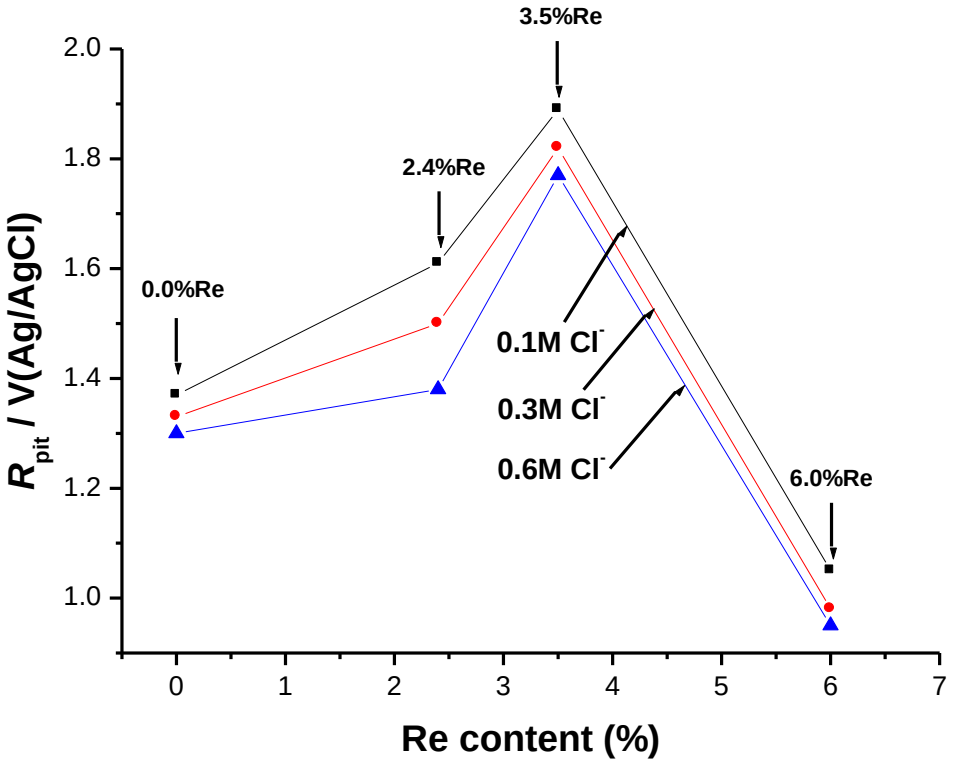

Figure 10. Dependence of the pitting corrosion resistance (R_{pit}), expressed in volts, recorded for the tested alloys in 1.0 M H_2SO_4 solutions containing different concentration of Cl^- at room temperature, on the percentage of alloyed Re content.

3.3.1.2. Potentiostatic measurements

Potentiostatic current *vs.* time measurements were also carried out to gain more information concerning the effect of alloyed Re on the kinetics of pitting corrosion of the tested alloys in Cl^- containing – H_2SO_4 solutions. Measurements were conducted at various anodic potentials as a function of Cl^- concentration. Figure 11 displays the current *vs.* time plots recorded for the tested alloys in 1.0 M H_2SO_4 solution at an applied anodic potential of E_a = 0.5V at 25 ^oC.

It follows from Fig. 11 that, in the absence of Cl^-, the transient current profile can be divided into two stages. In the first stage, the anodic current transient decreases rapidly with time, due to the electroformation and growth of a passive oxide film on the anode surface.

The anodic current of the second stage (steady-state current, j_{ss}) was nearly constant irrespective of applied potential, indicating that the rate of oxide formation equals that rate of oxide dissolution so that the oxide film hardly grows [36-38].

In such a case, the overall transient current density can be related to two main processes, namely the passive layer growth (j_{gr}) and metal electrodissolution through the passive layer (j_{dis}), Eq. 8.

$$j = j_{gr} + j_{dis} \quad (8)$$

The growth of the passive layer can be assigned to the formation of a passive oxide solid phase on the electrode surface. The electrodissolution of the anode through the passive layer can be explained in terms of cation diffusion from the metal/film interface to the film/solution interface. These two processes can proceed independently on the entire electrode surface. It seems that the rates of these two processes are nearly the same at the steady-state current so as to keep the thickness of the passive film nearly constant.

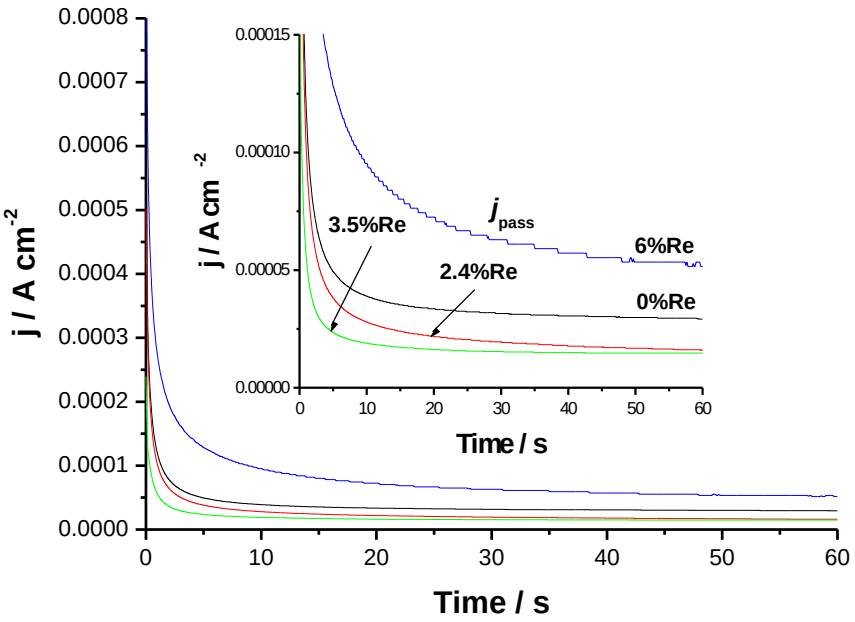

Figure 11. Current *vs.* time plots recorded for the tested alloys in 1.0 M H_2SO_4 solution at an applied anodic potential of E_a = 0.5V at 25 ^oC.

It is observed that the value of j_{ss} decreases, corresponding to a more protective passive oxide film, as alloyed Re content increases up to 3.5%. On the other hand, the value of j_{ss} enhances when our tested Inconel is alloyed with 6.0% Re, reflecting the formation of a less protective (thin and/or porous) passive film.

On the other hand, in presence of Cl^- (Fig. 12), it can be seen that the overall process is categorized into the three stages, i.e. the first passivation stage, the second pit formation and growth stage and the final steady-state stage.

The anodic current density of the first stage descended abruptly with time and then reached a current minimum at a certain incubation time, t_i (well defined in the insert of Fig. 12). The incubation time is caused by the time required for local removal of the passive film via the sequence of Cl^- adsorption, penetration and formation of soluble complexes. The fall of current density indicates thickening of oxide film on the surface. In the second stage, the value of current density ascended from the moment just after t_i to another time designated here as τ, which is attributed to passivity breakdown induced by the aggressive attack of Cl^-, and subsequent formation and growth of pits.

Within the 2nd stage, the general trend of an increasing current suggests that pit growth is the dominant process and a number of well-developed pits could be observed following this active period. In this case, the overall transient current density is given by three contributions, Eq. 9, with j_{pit} being related to the pit growth current density.

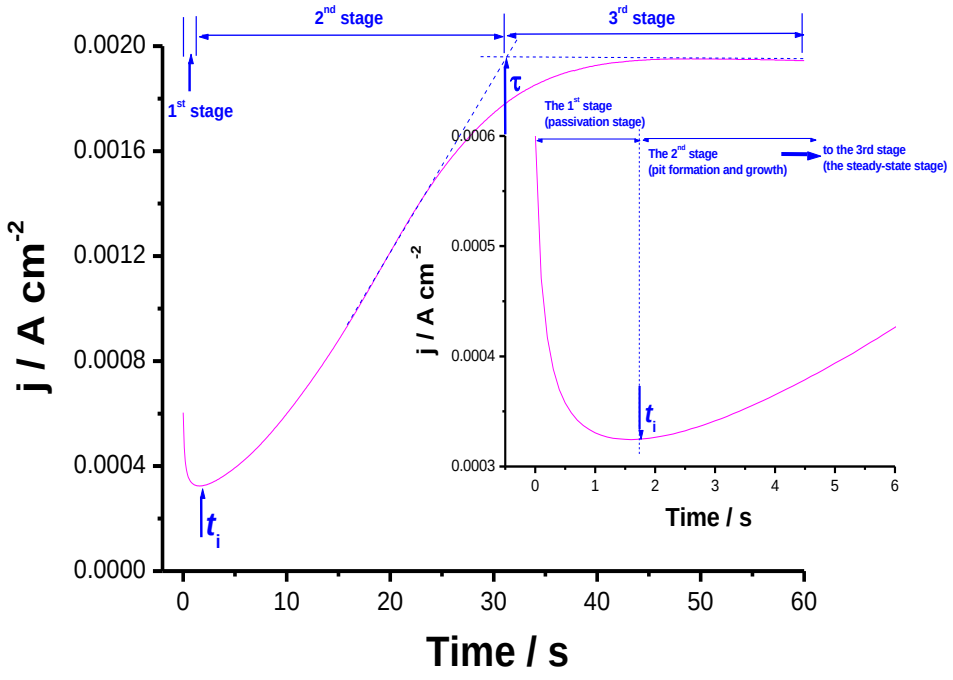

Figure 12. A current *vs.* time plot recorded for (IN718–2.4%Re) alloy in (1.0 M H_2SO_4 + 0.6 M NaCl) solution at E_a = 0.5V at 25 ^oC.

$$j = j_{gr} + j_{dis} + j_{pit} \quad (9)$$

After pit initiation, see the current rise between t_i and τ, it is possible that pitting corrosion products precipitate inside the pits. The corrosion products block up the pits, and therefore hinder the current flow through the pits. Thus, a steady-state was attained between the metal dissolution and

oxide film formation including a blockade by pitting corrosion product in the third stage of current transient after τ. Similar findings were previously obtained in our lab during pitting corrosion (induced by SCN^- [29]) studies of Al and Al-Zn alloys.

In the third stage, the increment in current density caused due to the metal dissolution just equals the sum of the decrement in current density due to oxide film formation and the decrement of current density due to the blockade by pitting corrosion product, leading to nearly constant current density.

Further experiments were performed to clarify the influence of C_{Cl^-} on the current transients of each tested sample at various anodic potentials at 25 ^oC. Some of the obtained results are depicted in Fig. 13, which shows the effects of C_{Cl^-} and E_a on the current transients of (IN718–2.4%Re) alloy in 1.0 M H_2SO_4 at 25 ^oC. Similar findings were obtained for the other tested alloys (data not shown here).

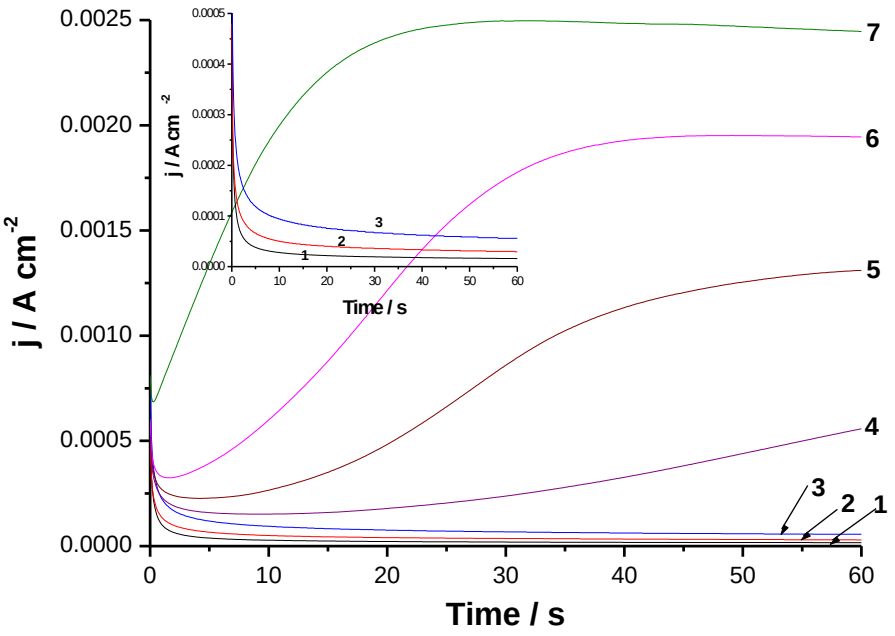

Figure 13. Current *vs.* time plots recorded for (IN718–2.4%Re) alloy in 1.0 M H_2SO_4 solutions containing various concentrations of Cl^- as a function of E_a at 25 ^oC. Curves 1-5 were recorded at E_a = 0.5V, while curves 6 and 7 were monitored at E_a = 0.6V and 0.8V, respectively. **(1)** 0.0M Cl^-; **(2)** 0.01M Cl^-; **(3)** 0.1M Cl^-; **(4)** 0.3M Cl^-; **(5-7)** 0.6M Cl^-

The obtained experimental findings revealed that t_i and τ vary with C_{Cl^-} and E_a, being shorter, corresponding to increased susceptibility towards pitting corrosion, with increasing C_{Cl^-} and E_a.

The content of alloyed Re in our IN718 also had an influence on the kinetics of pit formation and growth. The incubation time is found to increase with increase in Re content (up to 3.5%Re), while it decreased when IN718 alloyed with 6%Re. These results reveal that there is a growing tendency that the rate of passivation dominates over the rate of oxide dissolution as alloyed Re increased up to 3.5%, resulting in an obvious increase in t_i. On the contrary, further increase in Re content, as in the case of IN718-6%Re alloy, has resulted in an obvious decrease in t_i.

To clarify these findings and conclusions, the rate of pit initiation, defined as t_i^{-1}, is plotted as a function of C_{Cl}^-, E_a and Re content, see Fig. 14.

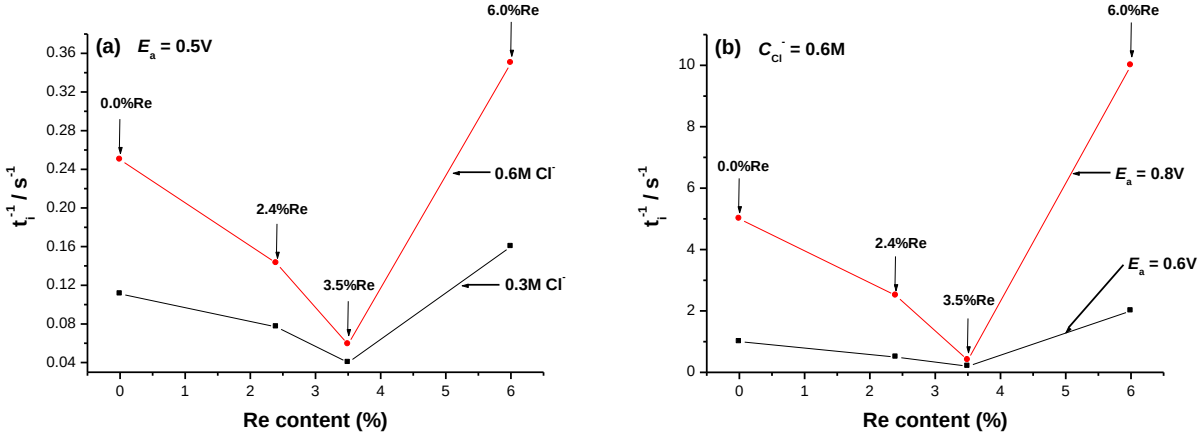

Figure 14. Dependence of the rate of pit initiation (t_i^{-1}) on Re content as a function of **(a)** C_{Cl}^- at E_a = 0.5V and **(b)** E_a at C_{Cl}^- = 0.6M.

It is obvious that the rate of pit initiation enhances, for any tested alloy, with C_{Cl}^- and E_a, while it decreases, at any fixed value of C_{Cl}^- or E_a, with increase in %Re (up to 3.5%). Alloying IN718 with 6%Re recorded the highest rate of pit initiation among the tested samples at any given value of C_{Cl}^- or E_a. These findings confirm and go parallel with the results of potentiodynamic anodic polarization measurements.

3.5. Role of alloyed Re

The role played by alloyed Re, 2.4% and 3.5% (and except for 6.0%Re), in improving the pitting corrosion resistance of our tested IN718 in these solutions may be explained from the corrosion point of view, as follows. Any localized dissolution will preferentially dissolve the base metal (Ni) and leave the surface enriched in unreactive Re atoms, as evidenced from ICP-AES measurements. Such method of chemical analysis showed that the amount of Ni released in the solution after any pitting corrosion test decreased when the percentage of the alloyed Re increased in the alloy from 0 to 2.4 and from 2.4 to 3.5, but drastically increased in presence of 6.0% of alloyed Re.

Enrichment of alloy surface in unreactive Re atoms during dissolution blocks the active sites available for Ni dissolution. At this stage, dissolution is retarded and pitting ceases. In order for pitting to recommence, the potential must be raised even higher [to $(E_{pit})_{alloy}$] to activate dissolution at the less favourable sites. As the Re content is increased (up to 3.5%), Re atoms will appear with greater frequency. Therefore, dissolution processes will be retarded until increasingly higher potentials are reached. Therefore, $(E_{pit})_{alloy}$ must increase with Re content, as shown in Fig. 8.

The high corrosion resistance of Inconel-2.4%Re and Inconel-3.5%Re alloys, compared with Re free-Inconel alloy, can also be attributed to the incorporation of Re atoms in the passive film covering the alloy surface, as confirmed from EDS analysis. This incorporation is expected to repair

the film defects and precludes significant dissolution of the oxide film. This makes it more difficult for Cl^- to migrate through the passive oxide film. Alloyed Re would as a result increase the difficulty of soluble film formation required for film rupture to occur [39]. All these events are assumed to be more effective in improving pitting corrosion resistance when the alloyed Re content increased in the alloy from 2.4% to 3.5%.

The role played by Re as an alloying element in enhancing the pitting corrosion resistance of the tested IN718 alloy can also be explained adopting the microstructure studies of Re-containing IN718 alloys, previously published by N. El-Bagoury et al. [27,28]. El-Bagoury et al. reported that the solidification process starts with precipitation of primary γ phase, which is followed by interndendritic (γ+ NbC) and (γ+ Ni_2Nb) phases. Moreover, the volume fraction of the primary γ is increased, while the volume fraction of eutectic (γ+ NbC) and (γ+ Ni_2Nb) are decreased by the addition of Re. Also, increasing Re content enlarges the secondary dendrite arm spacing (SDAS).

The corrosion resistance ST IN718 alloy was enhanced by the addition of 2.4 and 3.5% of Re, however the addition of 6% of Re deteriorates the corrosion resistance of the ST IN718 alloy. The correlation between the Re additions to ST IN718 alloy and its corrosion resistance can be interpret by the area ratio between γ dendrites and inetrdendritic regions. As the Re content in creased in the IN718 alloy the volume fraction of γ dendrites increased on the account of interndendritc regions [27,28]. The critical ratio achieved with the addition of 6% Re leading to sever corrosion in interdendritic regions.

It may be of interest to note, however, that alloying our tested Inconel with 6% Re has resulted in an obvious increase in the rates of uniform and pitting corrosion processes. This behavior does not appear to have been reported in the literature, but it was a reproducible phenomenon in the present work, and has no clear explanation at the present time. Therefore, this point deserves further complementary studies.

4. CONCLUSIONS

The electrochemical and corrosion behavior of a standard Inconel 718 alloy (IN718), without and with various percentages (2.4, 3.5, and 6.0%) of Rhenium (Re) as an alloying element, has been studied in 1.0M H_2SO_4 solutions, based on various electrochemical techniques, complemented with SEM/EDS and AFM examinations. Monitoring open-circuit potential (OCP) studies revealed that the tested alloys tend to passivate in H_2SO_4 solutions, and the extent of passivation depends on %Re. The passivation rate is found to increase following the order: IN718-6%Re < IN718 < IN718-2.4%Re < IN718-3.5%Re. The alloy IN718-6%Re recorded the lowest passivation rate among the tested alloys, reflecting a more active corrosion surface of IN718-6%Re alloy when compared with IN718. This difference was attributed to the acceleration influence (harmful effect) of the alloyed Re, when increased to 6%. EIS spectra measured at E_{corr} came to the same conclusion and showed that the total impedance (Z) increases with increase in Re content up to 3.5%, then decreases when the content of Re has increased up to 6%. In this respect, the alloy with 3.5%Re recorded the highest Z, while that alloyed with 6.0%Re recorded the lowest value for Z. The Rate of uniform corrosion was estimated form Tafel extrapolation method as a function of alloy composition. The obtained results showed that

the uniform corrosion rate decreased when Re content increased from 2.5% to 3.5%, but enhanced with further increase in alloyed Re content (up to 6%).

The anodic behavior of the tested alloys was also studied in 1.0M H_2SO_4 solutions without and with Cl^-, based on potentiodynamic anodic polarization and potentiostatic (current *vs.* time measurements at a given potential) techniques. Experimental findings revealed that the susceptibility of IN718 alloy towards pitting attack (induced by Cl^-) was suppressed when the percentage of the alloyed Re was increased up to 3.5%, but enhanced in presence of 6.0% of alloyed Re. The 3.5%Re-containing IN718 alloy presented the highest pitting corrosion resistance (R_{pit}), while the lowest R_{pit} value was recorded for the IN718-6.0%Re alloy. Morphological studies of the corroded surfaces, based on SEM and AFM examinations, revealed that the severity of corrosion decreased with increase in alloyed Re content (up to 3.5%) in the test samples. However, further increase in Re content (6.0%) promoted corrosion. ICP-AES method of chemical analysis came to the same conclusion and confirmed electrochemical and morphological studies.

ACKNOWLEDGEMENT
The authors acknowledge the financial aid received from Taif University, Saudia Arabia (Project No. 1/434/1954).

References

1. High-Performance Alloys, *Special Metals Corporation* (SMC). http://www.specialmetals.com/products/index.php. Retrieved 2010=04=26.
2. "Special Metals Corporation (SMC): History". http://www.specialmetals.com/history.php. Retrieved 2012-05-18.
3. A. Devillez, G. Le Coz, S. Dominiak, D. Dudzinski, *J. Mat. Proc. Tech*., 211 (2011) 1590-1598.
4. W-S Lee, C-F Lin, T-H Chen, H-W Chen, *Mat. Sci. and Eng.* A, 528 (2011) 6279-6286.
5. K.H. Song, W.Y. Kim, K. Nakata, *Mat. & Des.*, 35 (2012) 126-132.
6. R. Damodaram, S. Ganesh Sundara Raman, K. Prasad Rao, *Mat. Sci. and Eng*. A, 560 (2013) 781-786.
7. J. Liu, J. Cao, X. Lin, X. Song, *J. Feng, Mat. & Des*., 49 (2013) 622-626.
8. R.G. Thmpson, D.C. Mayo, B. Radhakrishnan, *Metall. Trans*. A, 22 (1991) 557.
9. Q. Chen, N. Kawagoishi, H. Nisitani, *Mater. Sci. Eng*. A, 277 (2000) 250.
10. L. Nastac, D.M. Stefanescu, *Metall. Mater. Trans*. A, 27 (1996) 4075.
11. M.J. Cieslak, T.J. Headley, G.A. Knorovsky, A.D. Romig, T. Kollie, *Metall. Trans*. A, 21 (1990) 479.
12. J. Prybylowski, R. Ballinger, *Nat. Assoc. Corr. Eng*., 43 (1987) 111.
13. C.A. Huang, T.H. Wang, C.H. Lee, W.C. Han, *Mater. Sci. Eng.* A, 398 (2005) 275.
14. H.J. Jang, C.J. Park, H.S. Kwon, *Electrochim. Acta*, 50 (2005) 3503.
15. G. Frankel, *J. Electrochem. Soc*., 145 (1998) 2186.
16. O.M. Magnussen, J. Scherer, B.M. Ocko, R.J. Behm, *J. Phys. Chem*. B, 104 (2000) 1222.
17. N. Pineau, C. Minot, V. Maurice, P. Marcus, *Electrochem. Solid-State Lett*., 6 (2003) B47.
18. A.Bouzoubaa, B. Diawara, V. Maurice, C. Minot, P. Marcus, *Corros. Sci*., 51 (2009) 2174.
19. S. Singh, S. Basu, A.K. Poswal, R.B. Tokas, S.K. Ghosh, *Corros. Sci.*, 51 (2009) 575.
20. T. Nickchi, A. Alfantazi, *Corros. Sci*., 52 (2010) 4035.
21. Nader El-Bagoury, Adel A. Omar, K. Ogi, *Metallogr. Microstruct. Anal*. (2012) 1:35–44.

22. J.R. Vilche, A.J. Arvia, *Corros. Sci.* 15 (1975): p. 419-431.
23. E. McCafferty, Validation of corrosion rates measured by the Tafel extrapolation method, *Corros. Sci.* 47 (2005) 3202.
24. ASTM G 102 – 89 (Reapproved 1999), Standard Practice for Calculation of Corrosion Rates and Related Information from Electrochemical Measurements.
25. N. El-Bagoury, M.A. Amin, Q. Mohsen, *Int. J. Electrochem. Sci.*, 6 (2011) 6718.
26. J.R. Vilche, A.J. Arvia, *Corros. Sci.*, 15 (1975) 419.
27. Nader El-Bagoury, Kauro Yamamoto, Hirofumi Miyahara and Keisaku Ogi, *Materials Transactions* 46 (2005) 5: 909.
28. N. El-Bagoury, K. Yamamoto and Keisaku Ogi, *Materials Science and Technology* 21 (2005) 2: 204.
29. M.A. Amin, S.S. Abd El-Rehim, E.E.F. El-Sherbini, S.R. Mahmoud, M.N. Abbas, *Electrochim. Acta*, 54 (2009) 4288.
30. Metikos-Hukovic, R. Babic, Z. Grubac, S. Brinc, *J. Appl. Electrochem.*, 22 (1992) 325.
31. A. Kolics, J.C. Polkinghorne, A. Wieckowski, *Electrochim. Acta*, 43 (1998) 2605.
32. S.S. Abd El-Rehim, E. Hamed, A.M. Shaltot, M.A. Amin, *Z. Phys. Chem.*, 226 (2012) 59.
33. M.A. Amin, *Electrochim. Acta*, 54 (2009) 1857.
34. M.A. Amin, M.M. Ibrahim, *Compt. Rend. Chim.*, 14 (2011) 429.
35. S. Szklarska-Smialowska, Pitting Corrosion of Metals, D. 296, NACE, Houston, TX, 1986.
36. M.A. Amin, S.S. Abd El Rehim, S.O. Moussa, A.S. Ellithy, *Electrochim. Acta*, 53 (2008) 5644.
37. S.S. Abdel Rehim, H.H. Hassan, M.A. Amin, *Corros. Sci.*, 46 (2004) 1921.
38. M.A. Amin, S.S. Abdel Rehim, F.D.A.A. Reis, I.S. Cole, *Ionics*, 20 (2014) 127.
39. R.T. Foley, *Corrosion*, 42 (1986) 277.